SAND 96-1084C 7th Int. Conf. on Creep and Fracture of Eng. Materials + Structures

CONF-970803--2
SAND--96-1084C

ELEVATED TEMPERATURE CREEP PROPERTIES FOR SELECTED ACTIVE METAL BRAZE ALLOYS

J. J. Stephens

Senior Member of Technical Staff
Materials Joining Dept. (1833)
Sandia National Laboratories, Albuquerque, NM 87185-0367

ABSTRACT

Active metal braze alloys reduce the number of processes required for the joining of metal to ceramic components by eliminating the need for metallization and/or Ni plating of the ceramic surfaces. Titanium (Ti), V, and Zr are examples of active element additions which have been used successfully in such braze alloys. Since the braze alloy is expected to accommodate thermal expansion mismatch strains between the metal and ceramic materials, a knowledge of its elevated temperature mechanical properties is important. In particular, the issue of whether or not the creep strength of an active metal braze alloy is increased or decreased relative to its non-activated counterpart is important when designing new brazing processes and alloy systems.

This paper presents a survey of high temperature mechanical properties for two pairs of conventional braze alloys and their active metal counterparts: (a) the conventional 72Ag-28Cu (Cusil) alloy, and the active braze alloy 62.2Ag-36.2Cu-1.6Ti (Cusil ABA), and (b) the 82Au-18Ni (Nioro) alloy and the active braze alloy 82Au-15.5Ni-0.75Mo-1.75V (Nioro ABA). For the case of the Cusil/Cusil ABA pair, the active metal addition contributes to solid solution strengthening of the braze alloy, resulting in a higher creep strength as compared to the non-active alloy. In the case of the Nioro/Nioro ABA pair, the Mo and V additions cause the active braze alloy to have a two-phase microstructure, which results in a reduced creep strength than the conventional braze alloy. The Garofalo sinh equation has been used to quantitatively describe the stress and temperature dependence of the deformation behavior. It will be observed that the effective stress exponent in the Garofalo sinh equation is a function of the instantaneous value of the stress argument.

INTRODUCTION

Metal/ceramic brazing technology has been used for high voltage, high vacuum electronic devices for nearly three decades (1). In the most common

implementation of this technology, 94% alumina ceramic is metallized by the Mo-Mn process, followed by the electrodeposition of a Ni layer which supports wetting of the braze alloy. The metallic member - most often a controlled expansion alloy such as the Fe-29Ni-17Co (Kovar™) alloy or a low-expansion refractory metal such as Mo - is brazed to the ceramic under reducing conditions such as hydrogen or forming gas. Copper pinchoff tubes are also brazed into the device, which usually implies the use of step brazing processes for that and similar sub-assemblies. A number of parameters influence successful implementation of this brazing technology: braze joint geometry, materials and selection based on braze alloy mechanical and physical properties, and control of brazing process parameters are all needed to insure good product. Ceramic cracking problems can arise from creep strengthening of the alloy during overbrazing (2,3), the use of braze alloys which order during subsequent processing (4), and excessively rapid cooldown profiles that raise residual stresses in the ceramic (5). The lack of data for high temperature creep and tensile properties of braze alloys had previously limited the usefulness of Finite Element Analysis (FEA) calculations of residual stresses in brazed metal/ceramic assemblies. However, as will be discussed in this paper, a number of braze alloys have been investigated, and creep/plasticity models, which are useful for FEA calculations, have been developed (6).

Conventional metal/ceramic brazing - as described above - is often criticized for the relatively large number of processing steps needed to realize a final product. This has motivated a number new approacheds in recent years, including the use of diffusion bonded or braze shut devices that can eliminate pinchoff tubes. Active metal brazing simplifies brazing processes by eliminating the metallize and nickel plating normally used on alumina ceramics for hermetic joints. However, active metal brazing also raises some new technical issues, including problems with fixturing (active braze alloys also wet fixture materials and may necessitate redesign of fixturing). In addition, the question must be considered whether the active braze addition leads to strengthening of the braze alloy with the consequence of increase residual stresses in the joint members. The number of process steps saved by active metal brazing will not be realize an advantage if it causes higher frequencies of ceramic cracking due to large increases in braze alloy strength.

The mechanical properties described in this paper were generated in support of development programs at Sandia to evaluate the strength of active braze alloys with the ultimate goal of using these specific alloys in component and hardware applications. In the interest of conserving space, we will not discuss the microstructures of deformed samples in any detail, nor present complete tabulations of the data generated. This information will be made available in the near future in the form of refereed journal articles .

MATERIALS AND TESTING PROCEDURES

All of the materials used in this investigation were supplied by WESGO, Inc., Belmont, CA. Tables 1 and 2 show the chemical composition of each alloy based on chemical analyses furnished by the supplier at the time of purchase. For the case of Cusil and Cusil ABA alloys, all material was

stabilized by annealing at 750°C - 64 hr. and 168 hr., respectively - then swaged at room temperature to approximately 39% RA. The as-swaged material was annealed at 750°C for 2 hr. prior to machining into compression samples measuring 6.35 mm diameter by 12.7 mm high.

The Nioro and Nioro ABA alloys were procured in the form of 3.18 mm diameter rod and were machined into miniature tensile specimens as described in ref. 7.

Table 1

Chemical composition (wt.%) of Cusil and Cusil ABA materials

Alloy	Ag	Cu	Ti	Al	Zn	Pd
Cusil	71.20	28.80	-----	<0.0001	0.0004	0.0005
Cusil ABA*	62.24	36.2	1.56	0.060	0.0004	0.0010

* additional trace elements reported for Cusil ABA: **Mg** <0.0002; **Fe** 0.0030; **Ni** 0.0050; **Au** 0.0020; **Pb** not detected; **Mn** 0.0020; **Si** 0.0060 and **Y** 0.0030.

Table 2

Chemical composition (wt.%) of Nioro and Nioro ABA materials

Alloy	Au	Ni	Mo	V	Ag	Fe
Nioro*	81.69	18.31	----	----	0.0040	0.0030
Nioro ABA**	81.98	15.14	0.73	2.13	0.002	0.001

* additional trace elements reported for Nioro: **Al** 0.0003; **Mg** <0.001; **Mn** 0.0020; **Pd** 0.0070; **Cu** 0.03; **Si** 0.003; **In** 0.002.
** additional trace elements reported for Nioro ABA: **Mg** <0.0001; **Cu** 0.002; **Ca** 0.01; **Cr** 0.002; **Fe** 0.001; **Pb** <0.001.

Both Nioro and Nioro ABA alloys were annealed for 2 hrs. at 810°C, followed by water quenching. Since the Nioro alloy is prone to spinodal decomposition, these samples were then reheated to 810°C, held for 10 minutes, and then allowed to undergo a cooldown cycle based on a braze furnace cooldown (avg. cooling rate of 12°C/min.) to the intended testing temperature, water quenched, and then reheated and tested at that specific testing temperature. The Nioro ABA samples were determined to have a two-phase microstructure that is highly resistant to coarsening. As such, samples prior to testing were reheated to 810°C, held for 10 minutes, then allowed to cool to the test temperature at an avg. rate of 12°C/minute. In all tests, samples were held for 30 minutes at the testing temperature prior to application of load.

All testing and data collection were performed using a MTS servo-hydraulic testing system, equipped with Testar control. The specimens were heated using a Research Incorporated radiant heating furnace. The stress-strain curves were converted to true stress-true strain to permit determination of 0.2% yield stress and maximum true stress achieved in the test. For the

case of Nioro and Nioro ABA (run in tension), the uniform strain and strain to fracture were also obtained from the test data.

The Cusil and Cusil ABA samples were tested in compression using a compression cage fixture fabricated from a Ni base superalloy; samples were able to undergo deformation of about 0.18 to 0.20 eng. strain prior to the observation of significant barreling. The test strain was measured using an Inconel 601 extensometer attached directly to the top and bottom of the compression cage - this arrangement permitted strain determination across the platens with an LVDT mounted external to the heating zone. Two types of mechanical tests were run for these alloys: (a) constant true strain rate compression tests, run at 1.67E-4 s^{-1} (0.01/minute) and (b) constant load compression creep tests. The true strain rate compression tests were run prior to the creep tests at a given temperature to permit an estimation of the necessary stress levels for the subsequent creep tests. The stress-strain tests were run with the Testar system operating in "Playback mode" up to approximately 0.17 true strain in compression. The constant load compression creep tests used a constant loading rate of about 5 MPa/sec to permit controlled ramping up to the creep test load. Following the test, the minimum engineering strain rate was determined, and the true minimum strain rate and true stress were determined at the engineering strain point which constituted the midpoint of the strain range where the minimum creep rate was observed.

The Nioro and Nioro ABA alloys were studied using constant true strain rate tensile testing at three strain rates: 1.67E-6, 3.79E-5, and 8.33E-4 s^{-1}. At 700°C, testing was also performed at 1.83E-2 s^{-1} for the Nioro alloy only. Because of the relatively small sample size, the extensometer was attached to grooves that were machined in the sample grips, adjacent to where the samples were threaded in. Further details on the tensile sample testing are contained in Reference 7.

EXPERIMENTAL RESULTS

A. Cusil and Cusil ABA alloys

Compressive stress-strain curves for Cusil and Cusil ABA obtained at 250°C are shown in Figure 1. The data at 250°C, which were typical of the low temperature regime, from room temperature up to 450°C and indicate that Cusil ABA has generally higher yield and flow stress properties than the conventional Cusil alloy. The trends for yield stress and maximum compressive stress for both alloys as a function of temperature, obtained at a strain rate of 1.67E-4 s^{-1}, are shown in Figures 2 and 3, respectively. Cusil ABA is apparently strengthened by the addition of Ti, which segregates to the Cu-rich phase of the two-phase structure. To a limited extent, a third phase, apparently Cu_4Ti, is also observed. Electron microprobe analysis and wavelength dispersive X-ray maps confirmed this result (8).

It should also be noted in Figure 3 that above 600°C, Cusil ABA is relatively weaker than Cusil alloy. However, from the point of view of metal/ceramic brazing (2,5), the lower temperature mechanical properties are more important than those at the high homologous temperatures.

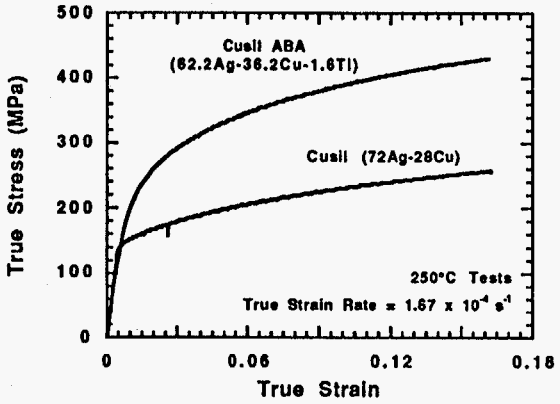

Figure 1. Compressive stress-strain curves for Cusil and Cusil ABA at 250°C.

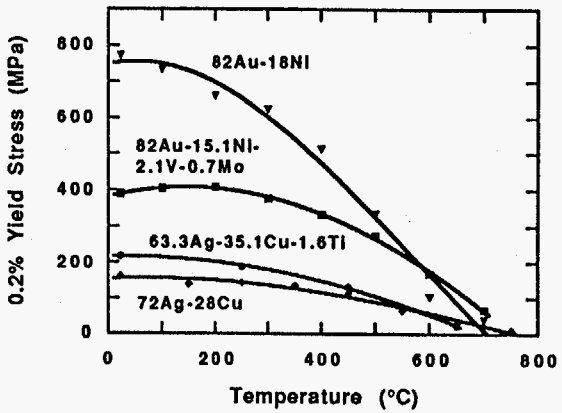

Figure 2. Yield stress vs. temperature for the four braze alloys.

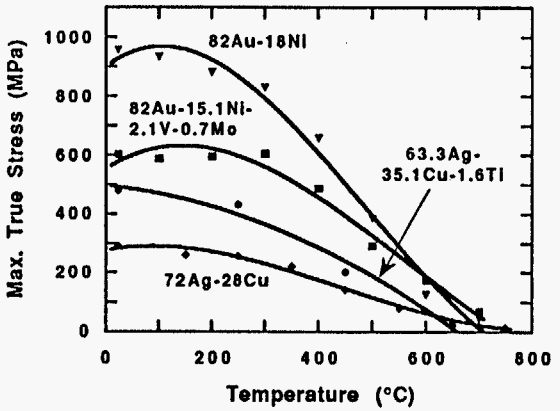

Figure 3. Maximum true stress vs. temperature for the four braze alloys.

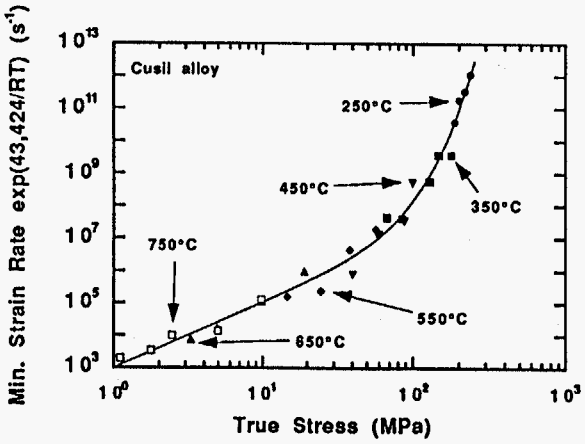

Figure 4. Comparison of data for swaged and annealed Cusil alloy vs. the fit to the data using eq. 2.

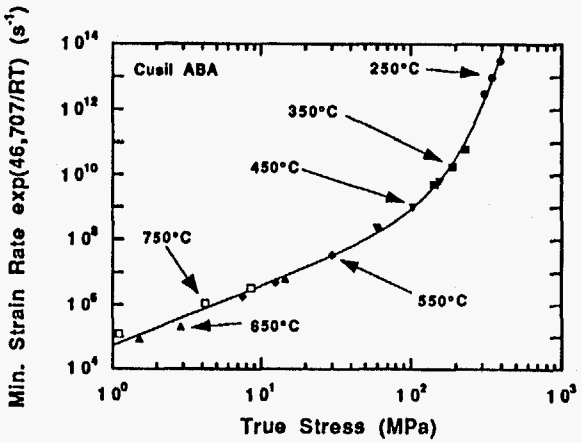

Figure 5. Comparison of data for swaged and annealed Cusil ABA vs. the fit to the data using eq. 3.

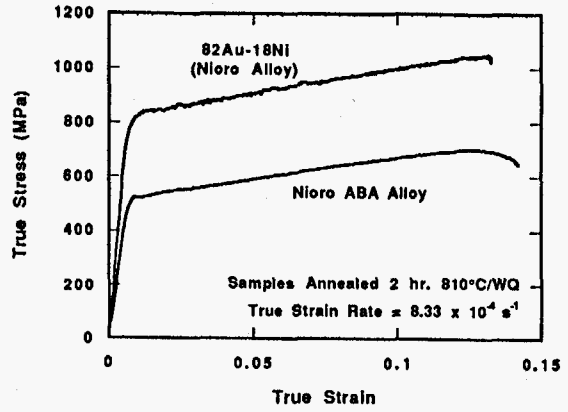

Figure 6. Comparison of room temperature tensile properties for Nioro alloy and Nioro ABA.

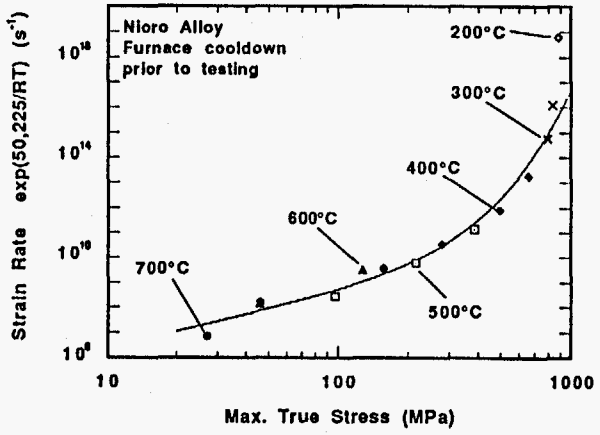

Figure 7. Comparison of data for annealed and furnace cooled Nioro alloy vs. the fit to the 300-700°C data using eq. 4.

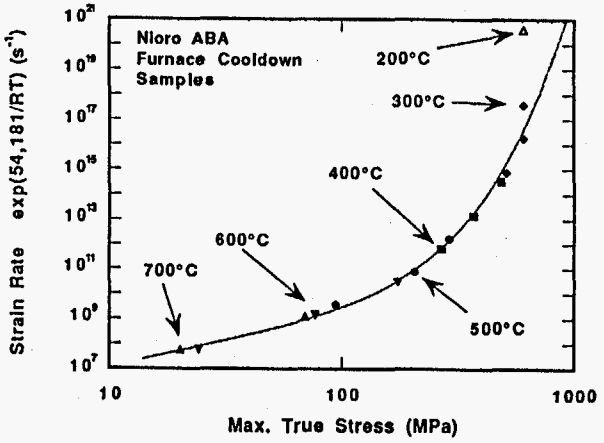

Figure 8. Comparison of data for annealed and furnace cooled Nioro ABA vs. the fit to the 300-700°C data using eq. 5.

The compressive creep data for both alloys over the temperature range 250-750°C were fit to the Garofalo sinh equation (9)

$$\dot{\varepsilon}_{min}\,(s^{-1}) = A\,[\sinh(\alpha\sigma(MPa))]^{n'}\exp-(Q_{cr}/RT) \qquad (1)$$

where n' is the apparent stress exponent, Q_{cr} is the activation energy for creep (cal/mole), T is the temperature in Kelvin, and R is the gas constant (1.987 cal/ mole-K). It should be noted that the apparent stress exponent, n', is not generally equal to the value of the effective stress exponent, n_{eff}, which is the actual slope of the curve on the log $\dot{\varepsilon}_{min}$ - log σ plot. By taking the natural logarithm of eq. (1) and iterating the value of $\alpha(MPa^{-1})$, the best least squares fit to the data were obtained - based on the r^2 parameter. The best fits to the Cusil and Cusil ABA alloys are as follows:

Cusil: $$\dot{\varepsilon}_{min}\,(s^{-1}) = 1.07E6\,[\sinh(0.03167\sigma)]^{2.019}\exp-(43{,}424/RT) \qquad (2)$$

Cusil ABA: $$\dot{\varepsilon}_{min}\,(s^{-1}) = 8.13E7\,[\sinh(0.01974\sigma)]^{1.867}\exp-(46{,}707/RT) \qquad (3)$$

These least-square fits had r^2 quality of fit parameters of 0.906 and 0.980 for Cusil and Cusil ABA, respectively. By shifting the Arrhenius term in eq. (1) to the left hand side of the equation, it is possible to show the creep data compared to the fit based on one master curve - in the manner of Zener and Holloman (10). The Zener-Holloman plots for both alloys are shown in Figures 4 and 5, respectively. Based on Figures 4 and 5, both sets of data indicate that the effective stress exponent n_{eff} is close to 2 at temperatures above 450°C, suggesting that grain boundary sliding controls the creep properties at these higher temperatures. However, at the lower temperatures, n_{eff} is much higher, suggesting a transition to climb-controlled processes in the so-called "power-law breakdown" regime.

Nioro and Nioro ABA Alloys

Unlike the Cusil/Cusil ABA materials, the Mo and V active metal addition to Nioro alloy to produce Nioro ABA results in a *decrease* in strength. A comparison of the room temperature stress-strain curves following a 2 hr./810°C anneal and water quench is shown in Figure 6. Note that the both the yield stress and flow stress is generally higher for Nioro alloy than for Nioro ABA; previous work (11) has also shown that the strain to fracture of Nioro is quite sensitive to hold times at 400°C - i.e., just within the region of spinodal decomposition on the Au-Ni phase diagram. Comparison of the yield stress (Figure 3) and maximum true tensile stress (i.e., the true stress equivalent of UTS), shown in Figure 4, also indicate that the Nioro alloy is substantially stronger than Nioro ABA alloy at temperatures up to 500°C. The data for Nioro alloy and Nioro ABA shown in Figures 3 and 4 were obtained at a strain rate of 8.33E-4 s^{-1}.

The microstructural reason for this decrease in strength (12) is that the additions of Mo and V in Nioro ABA apparently causes a stable two-phase microstructure to develop. The dominant volume fraction phase is a high Au phase with approximately 4.8 wt.% Ni; the entire Mo and V additions appear to segregate to the Ni-rich minor phase. On the other hand, Nioro alloy

solidifies as a single phase FCC alloy, that is prone to spinodal decomposition (along with increases in strength at intermediate temperatures (300-500°C). The strength of the two-phase Nioro ABA material is clearly limited by the low strength of the dominant Au-rich phase.

The maximum true stress data and strain rate data from 300-700°C were used for both alloys to construct a Garofalo sinh correlation. The 200°C tensile tests were found to consistently cause poor statistical correlations when included, thus they were omitted from the correlations. The Garofalo sinh correlation for Nioro alloy is as follows:

$$\text{Nioro alloy:}\quad \dot{\varepsilon}\,(s^{-1}) = 4.94E8\,[\sinh(0.00901\sigma_{max})]^{2.224}\exp\text{-}(50{,}225/RT) \quad (4)$$

with a correlation coefficient (r^2) equal to 0.880. The Zener-Holloman plot of this correlation is shown in Figure 7. The Garofalo sinh correlation for Nioro ABA was obtained:

$$\text{Nioro ABA:}\quad \dot{\varepsilon}\,(s^{-1}) = 4.88E8\,[\sinh(0.0161\sigma_{max})]^{2.002}\exp\text{-}(54{,}181/RT) \quad (5)$$

with a correlation coefficient (r^2) of 0.902. Figure 8 presents a comparison of the data and fit for Nioro ABA.

Discussion - Creep Activation Energies for Cusil and Cusil ABA

The values of Q_{cr} observed for Cusil and Cusil ABA were 43.4 and 46.7 kcal/mole, respectively. The activation energy for lattice self-diffusion in Ag, has been measured at 45.5 kcal/mole (13). Askill (13) has also tabulated the activation energy for tracer diffusion of Ag in Cu (46.5 kcal/mole) and that for Cu in Ag (46.1 kcal/mole). The activation enegy for lattice self-diffusion in pure Cu has two closely clustered accepted values - 47.1 and 49.6 kcal/mole. With all of these activation energies for bulk diffusion clustered within a range of about 10%, it is clearly not possible to infer additional insight regarding the measured values of Q_{cr} for the Cusil and Cusil ABA alloys - except to note that the values obtained from the least-squares procedure appear to be consistent with those from potential diffusion processes in the Ag-Cu binary system.

Discussion - Creep Activation Energies and Stress Exponents for Au-Ni Alloys

It is interesting to compare the values of Q_{cr} and n' obtained for Nioro and Nioro ABA alloys with some of the results for Au-Ni alloys generated by Sellars and Quarrell (14). Table 3 shows the power law stress exponent and Q_{cr} values obtained by Sellars and Quarrell. Creep correlations for pure Au obtained from a recent analysis of literature data (15), are also included.

Table 3

Activation Energy and Stress Exponent Values for Au-Ni Alloys, Pure Ni and Pure Au

Alloy (wt.%)	Type of Equation	Q_{cr} (kcal/mole)	n or n'	Temp. Range (°C)	Ref.
Pure Au	Power Law	50.6	5.65	820-940	14
90.8Au-9.2Ni	Power Law	60.5	3.27	820-940	14
76.4Au-23.5Ni	Power Law	57.2	2.96	820-940	14
Pure Ni	Power Law	66.2	5.65	820-940	14
Pure Au	Power Law	48.3	5.49	820-940	15
Pure Au	Garofalo sinh	24.1	3.06	395-500	15
Nioro	Garofalo sinh	50.2	2.22	300-700	this work
Nioro ABA	Garofalo sinh	54.2	2.00	300-700	this work

The values of Q_{cr} for Au-Ni alloys and Ni are clearly higher than that of pure Au - this would be expected based because the melting point of Ni is higher than that of Au. The activation energies observed in the tensile testing of Nioro and Nioro ABA are reasonably consistent with the other high temperature correlations shown in Table 3. For the case of pure Au at intermediate temperatures (395-500°C), dislocation core diffusion acts as a short circuit to lattice self-diffusion. Another important item to note in Table 3 is that the stress exponents for the Au-Ni alloys are close to 3 - because Au-Ni is considered a Class I solid solution alloy based on the relative size of the Au and Ni atoms (10). Thus, the source of the low values of n' observed for Nioro and Nioro ABA in the present invetigation could be due to the Class I solid solution effect when Ni is added to Au. However, the fact that the values of n' obtained with the Garofalo sinh law are lower than 3 must be interpreted with caution, as discussed in the next section.

Discussion - n_{eff} for the Garofalo sinh Equation

It should be noted that the effective stress exponent, n_{eff}, for the Garofalo sinh equation (i.e., the slope of the log ε_{min}-log σ plot) depends on the instantaneous value of the stress argument, $\alpha\sigma$. By taking the natural log of both sides of eq. 1 and then differentiating, it can be shown that

$$n_{eff} = n' (\alpha\sigma \coth(\alpha\sigma)) \qquad (6)$$

The ratio n_{eff}/n' is plotted as a function of as in Figure 9. Clearly, at low values of as, the value of n_{eff} is equal to n'. However, as $\alpha\sigma$ goes >>1, the value of n_{eff} increases linearly with $\alpha\sigma$, since $\coth(\alpha\sigma)$ tends to 1. This stress dependence for n_{eff} makes it somewhat difficult to compare stress exponents obtained with a power law equation with those from the Garofalo sinh equation. For example, with Nioro over the range of stress studied, n_{eff} varies from 2.22 at the lowest stresses up to 4.22 at 200 MPa, and a high of 17.0 at the highest stresses shown in Figure 7. Similarly, for Nioro ABA over the range of stresses studied, n_{eff} varies from 2.00 at the lowest stresses

up to 6.44 at 200 MPa, and a high of 19.3 at the highest stresses shown in Figure 8.

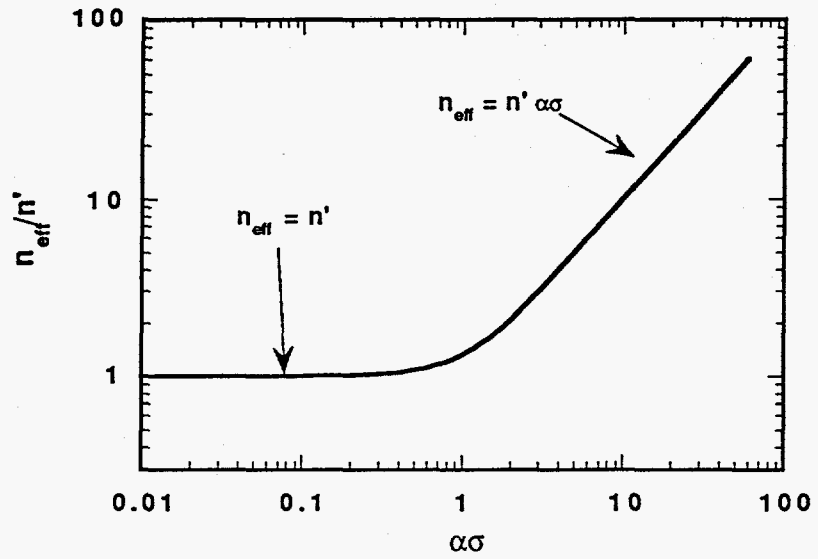

Figure 9. Plot of n_{eff}/n', to illustrate the dependence of n_{eff} on the instantaneous value of $\alpha\sigma$ in the Garofalo sinh equation (eq.1).

SUMMARY

1. The addition of Ti to the Cusil braze alloy to produce the active metal alloy, Cusil ABA, results in significant material strengthening, as measured in both compressive creep and monotonic, compressive stress-strain tests.

2. The addition of Mo and V to Nioro to produce Nioro ABA results in a net decrease in tensile properties - due to the stabilization of a two-phase microstructure.

3. The compressive creep data for Cusil and Cusil ABA, and the tensile stress-strain data for Nioro and Nioro ABA, can be fit to the Garofalo sinh equation. An analysis of the stress dependence of the effective stress exponent when the Garofalo sinh equation is used has also been presented.

ACKNOWLEDGMENTS

I would like to acknowledge the help of D. T. Schmale, T. Rice and K. D. Hamann, who performed the mechanical testing discussed in this paper. I would also like to acknowledge the able machining work of M. J. Mead, who produced the miniature tensile samples for this paper, and P. T. Vianco, for

reviewing this paper. This work was conducted at Sandia National Laboratories, supported by U.S. Dept. of Energy under contract number DE-AC04-94AL85000.

REFERENCES

1. W. H. Kohl, Handbook of Materials and Techniques for Vacuum Devices. New York: Rheinhold Publising, 1967. pp. 441-475.
2. J. J. Stephens, S. N. Burchett and F. M. Hosking, "Residual Stresses in Metal/Ceramic Brazing: Effect of Creep on Finite Element Analysis Results," in P. Kumar and V. A. Greenhut (eds.), Metal-Ceramic Joining Warrendale, PA: TMS, 1991. pp. 23-41.
3. J. J. Stephens and P. F. Hlava, "Reducing Inadvertent Alloying of Metal/ Ceramic Brazes," in J. J. Stephens and D. R. Frear (eds.), Low Thermal Expansion Alloys and Composites. Warrendale, PA: TMS, 1994. pp. 59-77.
4. J. Wittenauer, Lockheed Missiles and Space Co., Inc., Palo Alto, CA, private communication, June, 1990.
5. J. J. Stephens, S. N. Burchett and W. B. Jones, "Stress Relaxation of Braze Joints," in W. T. Chen and H. Abe (eds.), Advances in Electronic Packaging, 1992. New York, NY: ASME, 1992. pp. 363-372.
6. M. K. Neilsen, S. N. Burchett, C. M. Stone and J. J. Stephens, "A Viscoplastic Theory for Braze Alloys," SAND96-0984, Sandia National Laboratories, New Mexico (April, 1996).
7. J. J. Stephens and F. A. Greulich, "Elevated Temperature Creep and Fracture Properties of the 62Cu-35Au-3Ni Braze Alloy," Metallurgical Transactions, 26A, 1471-1482 (June, 1995).
8. J. J. Stephens, F. M. Hosking and S. N. Burchett, "Creep Properties of the 62.2Ag-36.2Cu-1.6Ti Active Metal Braze Alloy," talk presented at the 1993 Annual TMS Meeting, Denver, CO, February, 1993.
9. F. Garofalo, Fundamentals of Creep and Creep-Rupture in Metals, New York, NY: The MacMillan Company, 1965. pp. 51-55.
10. O. D. Sherby and P. M. Burke, "Mechanical Behvior of Crystalline Solids at Elevated Temperature," Progress in Materials Science, 13, 325-390 (1967).
11. J. J. Stephens and K. D. Hamann, "High Temperature Tensile Properties of the BAu-4 (82Au-18Ni) Braze Alloy," talk presented at the 1994 Annual TMS Meeting, San Francisco, CA, February, 1994.
12. J. J. Stephens and K. D. Hamann, "The Effect of Vanadium Active Metal Addition on the Mechanical Properties of a Nickel-Gold Braze Alloy," talk presented at the 1995 Annual TMS Meeting, Las Vegas, February, 1995.
13. J. Askill, Tracer Diffusion Data for Metals, Alloys, and Simple Oxides. New York: IFI/Plenum, 1970. pp. 32, 37, 45, 50.
14. C. M. Sellars and A. G. Quarrell, "The High Temperature Creep of Gold-Nickel Alloys," J. Inst. Metals, 90, 329-336 (1961-2).
15. J. J. Stephens, "Creep Correlations for Pure Au," Internal SNL memo, dated January 2, 1996.